Journal of *Marine Science and Engineering*

MDPI

Article

Vessel Trajectory Prediction Using Vessel Influence Long Short-Term Memory with Uncertainty Estimation

Zhiyuan Guo [1,2,*], Huimin Qiang [1,2] and Xiaodong Peng [2,*]

[1] University of Chinese Academy of Sciences, Beijing 100049, China; qianghuimin21@mails.ucas.ac.cn
[2] National Space Science Center, Chinese Academy of Sciences, Beijing 100190, China
* Correspondence: guozhiyuan19@mails.ucas.ac.cn (Z.G.); pxd@nssc.ac.cn (X.P.)

Abstract: Vessel trajectory prediction plays a crucial role in ensuring the safety and efficiency of maritime transportation. This study proposes an innovative sequence-to-sequence model, called the Vessel Influence Long Short-Term Memory (VI-LSTM), which introduces a novel Vessel Influence Map (VIM) to quantitatively model the dynamic effects of surrounding vessels. To enhance reliability, VI-LSTM incorporates Gaussian distribution predictions combined with Monte Carlo dropout techniques to estimate prediction uncertainty. Additionally, a temporally weighted hybrid loss function is designed to balance prediction accuracy and uncertainty. Furthermore, this study systematically categorizes and models factors influencing vessel trajectory prediction. Experimental results demonstrate that VI-LSTM achieves a mean distance error of 330.66 m on the standard test set and 480.30 m on an unseen subject test set, outperforming other comparative models, particularly in complex navigation scenarios and high-density maritime environments. These innovations significantly improve the accuracy and generalizability of vessel trajectory predictions, leading to enhanced safety, increased efficiency, and more effective collision avoidance in maritime navigation.

Keywords: trajectory prediction; vessel influence map; uncertainty estimation; multifactor prediction; temporally weighted hybrid loss function

check for updates

Academic Editor: Eugen Rusu

Received: 10 January 2025
Revised: 27 January 2025
Accepted: 13 February 2025
Published: 14 February 2025

Citation: Guo, Z.; Qiang, H.; Peng, X. Vessel Trajectory Prediction Using Vessel Influence Long Short-Term Memory with Uncertainty Estimation. *J. Mar. Sci. Eng.* **2025**, *13*, 353. https://doi.org/10.3390/jmse13020353

Copyright: © 2025 by the authors. Licensee MDPI, Basel, Switzerland. This article is an open access article distributed under the terms and conditions of the Creative Commons Attribution (CC BY) license (https://creativecommons.org/licenses/by/4.0/).

1. Introduction

Vessel trajectory prediction technology plays an indispensable role in enhancing maritime navigation safety and traffic management efficiency. This technology aids in preventing vessel collisions and offers decision-making support in domains such as route planning [1], port operations [2], and anomaly detection [3]. However, the unpredictability of vessel behaviors, complexity of marine environments, and dynamic interactions between vessels amplify the challenge of accurate trajectory prediction.

Recent years have seen significant advancements in vessel trajectory prediction performance [4,5]. However, most models focus on vessel motion and positional information while neglecting the effects of environmental factors and static characteristics of the vessel on its future trajectory. Moreover, insufficient research has been conducted on quantitative methods for calculating the effects of surrounding vessels on a target vessel. In addition, prediction uncertainty estimation is often overlooked.

To address these challenges, this study proposes a sequence-to-sequence (Seq2seq) model termed Vessel Influence Long Short-Term Memory (VI-LSTM). Unlike traditional LSTM-based approaches, VI-LSTM incorporates a novel Vessel Influence Map (VIM) to systematically quantify the dynamic influence of surrounding vessels on the prediction

target, enabling the model to better capture complex interactions and anticipate potential maneuvers. Additionally, it proposes a customized loss function that optimizes both prediction accuracy and uncertainty, enhancing the precision and reliability of vessel trajectory predictions. The primary contributions of this study are as follows:

1. Key factor modeling: This study provides a comprehensive analysis of the key factors influencing vessel trajectory prediction, which are categorized into vessel movement, environmental, vessel static, and surrounding vessel influence factors.
2. Vessel Influence Map (VIM): By introducing the VIM, the study provides a structured and quantitative framework for incorporating the influence of surrounding vessels into trajectory predictions. Unlike previous methods, VIM is grounded in COLREGs, ensuring compliance with maritime safety standards.
3. Loss function: This study proposes a temporally weighted hybrid loss function explicitly tailored to the vessel trajectory prediction problem. The loss function evaluates prediction accuracy using distance error metrics and quantifies prediction uncertainty by incorporating Monte Carlo (MC) Dropout estimates and modeling the predicted vessel positions as a Gaussian distribution.

The remainder of this paper is organized as follows. Section 2 reviews the development history of vessel trajectory prediction and identifies the shortcomings in existing research. Section 3 presents the theoretical basis of this study and details the model architecture. Section 4 demonstrates the effectiveness of our approach by presenting the results of comparative experiments and ablation studies. Finally, Section 5 summarizes the main findings of this study and directions for future research.

2. Related Work

Vessel trajectory prediction is significant for enhancing intelligent maritime transportation management systems. The development of this field can generally be divided into three stages, focusing on kinematic-based simulation methods, statistical and machine learning methods, and finally, deep learning-based methods [6,7]. This section reviews the developmental history of vessel trajectory prediction methods and the main limitations of the current research.

Research initially concentrated on the use of vessel physical models and kinematic equations for position prediction [8,9]. These physics-based methods provide a theoretical foundation for understanding basic vessel motion patterns but exhibit limitations when dealing with dynamic and complex interactions in busy maritime areas. Their primary deficiency is an inability to adapt to nonlinearities and variability, which leads to significant decreases in accuracy in complex scenarios.

Subsequently, statistical methods and machine learning-based approaches became the primary techniques in this field. Statistical methods [10–14] use manually designed data models to fit historical vessel trajectory data and predict future positions based on current states. Although these methods are effective in specific scenarios and constraints, they are challenging to apply universally and struggle to achieve precise results in complex and traffic-dense maritime regions.

Machine learning methods [15–18], which are known for their strong nonlinear fitting capabilities, have also been applied extensively to vessel trajectory prediction. Moreover, clustering technologies [19,20] have been employed for the linear or point clustering of trajectory data. Line clustering methods [21–23] have often been used for trajectory preclassification, followed by the training of refined models for different trajectory categories to enhance the prediction accuracy. Point clustering methods [20,24,25] have typically been used to extract key maritime waypoints and construct maritime traffic network models. These approaches estimate the next waypoint to determine the current route of the vessel

and thereby predict future trajectories, generally perform well in long-term trajectory prediction, and offer a degree of interpretability.

Deep learning models have gradually become the focus of vessel trajectory prediction research. These models can extract features from vast historical data automatically, identify complex patterns within trajectory data, and analyze time-series data effectively. Techniques such as convolutional neural networks [26,27], LSTM [28], bidirectional LSTM (BiLSTM) [29,30], bidirectional gated recurrent units [31,32], Seq2seq [33,34], generative adversarial networks [35,36], graph convolutional neural networks [37,38], and Transformer [39,40], along with various combinations and variants thereof, have been widely explored and used in experimentation by researchers. These methods have significantly improved the accuracy and reliability of short- and medium-term trajectory predictions in complex scenarios.

Despite the notable achievements of deep learning methods, the current research still has limitations. Most studies focus on using the longitude (lon), latitude (lat), speed over ground (sog), and course over ground (cog) for predictions and neglect other factors that could influence future vessel behavior. Therefore, we systematically collected and incorporated the key factors that affect the future trajectories of vessels. In addition, vessel behavior is significantly influenced by surrounding vessels when navigating in crowded waters. Understanding behaviors such as following, overtaking, and avoidance among vessels can help to improve the model prediction accuracy in complex environments. Thus, we designed a VIM model to capture the effects of surrounding vessels on the primary vessel. Finally, estimating the uncertainty of predictions is as important as achieving high prediction accuracy in deep learning-based vessel trajectory prediction tasks. Therefore, we developed an uncertainty estimation scheme that provides a confidence range for each prediction outcome.

In summary, vessel trajectory prediction has undergone extensive development and research. Based on an in-depth analysis of vessel trajectory prediction technologies, this work proposes improvements to enhance the accuracy, generalizability, and interpretability of vessel trajectory predictions.

3. Methodology

3.1. Problem Formulation

This study conceptualizes vessel trajectory prediction as a supervised learning task. We use the target vessel's historical motion data and surrounding environment from time 1 to T, along with static information, to generate the predicted trajectory sequence of the vessel from time $T+1$ to H. This prediction is performed using a deep model F (Figure 1), which can be expressed as

$$\hat{Y} = F(X, I; \theta) \tag{1}$$

where θ represents the model parameters. I is the static information of the target vessel (as detailed in Section 3.2.3). In addition, $X = [x_1, x_2, \ldots, x_T]$ is the historical temporal information from time 1 to T. For any given time t,

$$x_t = [P_t, E_t, VIM_t] \tag{2}$$

where P_t is the motion information of the target vessel at time t (as detailed in Section 3.2.1), E_t represents the environmental information at that moment (as detailed in Section 3.2.2), and VIM_t describes the information of surrounding vessels at that moment (as detailed in Section 3.3).

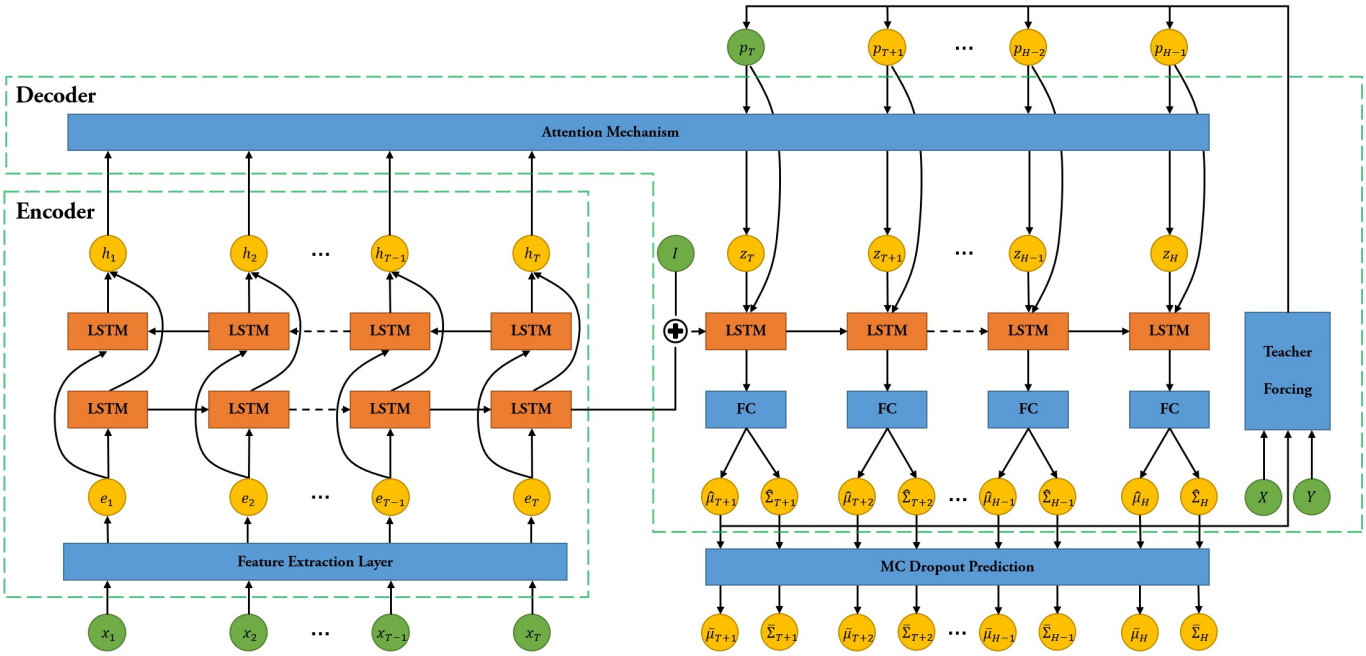


Figure 1. Schematic of the network structure for the Vessel Influence Long Short-Term Memory (VI-LSTM) with uncertainty estimation. Green circles: external input data; yellow circles: variables computed internally by the model; rectangles: computational processes or modules; arrows: direction of data flow.

In the prediction phase, the deep learning model extracts features from X and I and predicts the position probability distribution $\hat{Y}$ of the target vessel from time $T+1$ to H:

$$\hat{Y} = [\hat{y}_{T+1}, \hat{y}_{T+2}, \ldots, \hat{y}_H] \tag{3}$$

The prediction position $\hat{y}_t$ at any time t is

$$\hat{y}_t = [\mu_{lon,t}, \mu_{lat,t}, \sigma_{lon,t}, \sigma_{lat,t}, \rho_t] \tag{4}$$

which represents the predicted values of the mean lon, mean lat, standard deviation of lon, standard deviation of lat, and correlation coefficient between lon and lat.

The prediction position $\hat{y}_t$ for each moment can be represented as a multivariate Gaussian distribution $\mathcal{N}(\hat{\mu}_t, \hat{\Sigma}_t)$:

$$\begin{aligned} \hat{\mu}_t &= [\mu_{lon,t}, \mu_{lat,t}] \\ \hat{\Sigma}_t &= \begin{bmatrix} \sigma^2_{lon,t} & \rho_t \sigma_{lon,t} \sigma_{lat,t} \\ \rho_t \sigma_{lon,t} \sigma_{lat,t} & \sigma^2_{lat,t} \end{bmatrix} \end{aligned} \tag{5}$$

3.2. Key Factor Modeling

3.2.1. Vessel Motion Factors

We assume that the motion of a vessel follows physical laws and intrinsic motion patterns. Therefore, the future motion behavior will be affected by motion inertia. We would like the model to understand the motion pattern of the vessel over the past period as well as the relationship between this motion pattern and the future behavior. The historical motion information includes the lon, lat, sog, and cog. The lon and lat encompass the morphological patterns of the trajectory, whereas the sog and cog incorporate the changing rules of the motion.

We also include the *lon* and *lat* variations to describe the trajectory morphological features that are not related to the absolute position.

$$\Delta lon_t = \begin{cases} 0 & \text{if } t = 0, \\ lon_t - lon_{t-1} & \text{otherwise} \end{cases} \tag{6}$$

$$\Delta lat_t = \begin{cases} 0 & \text{if } t = 0, \\ lat_t - lat_{t-1} & \text{otherwise} \end{cases} \tag{7}$$

The *sog* and *cog* have a complex kinematic transformation relationship with the *lon* and *lat*. To facilitate learning of the correlation between these two types of features, we decompose the *sog* into the northward and eastward speeds using the *cog*:

$$\begin{aligned} v_{n,t} &= sog_t \cdot \cos(cog_t) \\ v_{e,t} &= sog_t \cdot \sin(cog_t) \end{aligned} \tag{8}$$

Therefore, we represent the vessel motion factors P_t of the target vessel at time t as

$$P_t = [lon_t, lat_t, \Delta lon_t, \Delta lat_t, v_{n,t}, v_{e,t}] \tag{9}$$

3.2.2. Environmental Factors

We selected the seawater depth and time state as the environmental factors in this study:

$$E_t = [depth_t, timeState_t] \tag{10}$$

Seawater depth is a critical consideration for maritime navigation safety. Based on the lat and lon at time t, we obtained the seawater depth information $depth_t$ from the GEBCO global bathymetry dataset[1].

Visibility differences in different time states can also affect the navigational behaviors of vessels. Hence, time state information also implies the periodic navigational patterns that are specific to certain regions. We divide the day into three time states based on different sunlight conditions: night (denoted by 0), day (denoted by 1), and dawn or dusk (denoted by 2). Based on the moment t and vessel coordinates, we calculate the solar altitude $altitude_t$. If the solar altitude is below $-15°$, the time state is considered to be night. If the solar altitude is above 15°, it is day. Otherwise, it is dawn or dusk. This is expressed by the following formula:

$$timeState_t = \begin{cases} 0 & \text{if } altitude_t < -15, \\ 1 & \text{if } altitude_t > 15, \\ 2 & \text{otherwise.} \end{cases} \tag{11}$$

Before inputting this information into the model, the time state is converted into a one-hot encoding form.

3.2.3. Vessel Static Factors

We consider the static factors of vessels, including the length, width, type, and MMSI:

$$I = [length, width, type, mmsi] \tag{12}$$

The length and width of a vessel directly affect its maneuverability. The size also determines the navigational restrictions of a vessel under specific conditions. Different

types of vessels have distinct operational characteristics and purposes, as well as different inherent motion patterns.

The MMSI enables the identification of specific vessels and their historical behaviors, which helps to provide contextual information for the prediction model.

Analyzing the correlations between static factors and other factors helps the model to understand the underlying decision-making reasons behind vessel trajectories, thus enabling the model to provide predictions that are closer to actual behavioral patterns under complex navigational conditions.

3.2.4. Surrounding Vessel Influence Factors

In busy maritime areas, vessel behaviors adhere to the COLREGs [41], as stipulated by the International Maritime Organization. The behaviors of surrounding vessels significantly influence the navigational choices of the target vessel.

We pre-extract the vessel motion factors P and static factors I of all vessels within an 8-nautical-mile range of the target vessel at moment t from the database. The motion factor P is processed according to Equation (8) to obtain the velocity components after orthogonal decomposition, whereas the static factors I retain only the vessel length and width.

In maritime navigational decision support systems, the distance to the closest point of approach (DCPA) and time to the closest point of approach (TCPA) are critical safety parameters used to assist navigators in determining when and how to take collision avoidance measures [42,43]. The DCPA is the closest distance that would be reached if both vessels were to maintain their current speed and course, whereas the TCPA is the time required to reach this closest distance [44].

Moreover, the traffic flow around the target vessel creates driving environmental pressure on the navigator, which restricts the operational behavior of the vessel [1]. The quantitative model for the driving environmental pressure between two vessels is

$$ST = 0.0019 \times d - 0.65 \times \ln(l_m) - \beta \tag{13}$$

where d represents the distance between the two vessels and l_m represents the average length of the two vessels. In addition, β is a regression coefficient that is adjusted according to the relative bearing of the vessels to reflect different stress impacts caused by approaches from different directions. When the approaching vessel is in direction A, B, or F, β = 2.07; in direction C or D, β = 0.85; and in direction E, β = 2.35 (Figure 2).

Ultimately, the influence of a surrounding vessel k on the target vessel at time t can be represented as

$$\begin{aligned} O_{t,k} = [&v_{n,t,k}, v_{e,t,k}, length_{t,k}, width_{t,k}, \\ &DPCA_{t,k}, TPCA_{t,k}, ST_{t,k}] \end{aligned} \tag{14}$$

3.3. VIM

Vessel trajectory prediction is complicated by the fact that the behavior of a vessel is determined by both its intrinsic motion patterns and the behaviors of surrounding vessels. However, traditional prediction methods often ignore such dynamic interactions between vessels, resulting in insufficient prediction accuracy in complex maritime environments. The social LSTM technique is an advanced method with which to address such challenges [45,46] in pedestrian trajectory prediction. Inspired by this method, we propose the VIM to enhance the ability of the model to understand the dynamic interactions between vessels via the quantitative modeling of the spatial distribution of surrounding vessels.

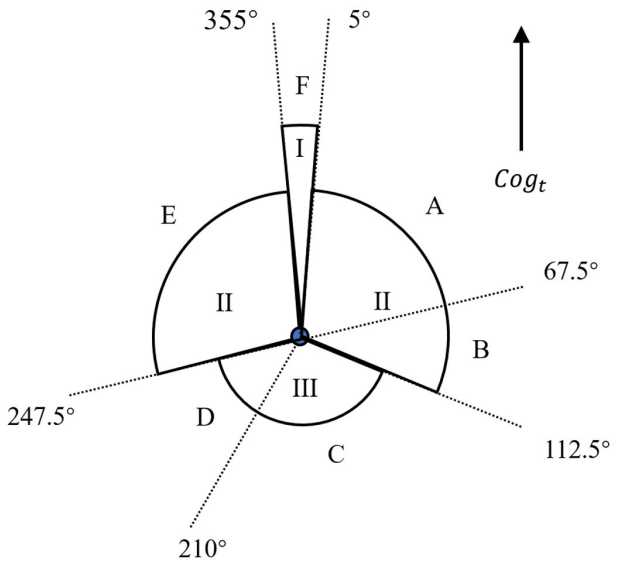


Figure 2. Schematic of the classification of vessel encounter patterns. The dotted lines in the diagram represent directional rays, with the adjacent numbers indicating the angles of these rays. A–F represent six different vessel encounter directions, while I–III indicate the zones of the three types of encounter patterns.

The VIM is based on the definition of vessel collision risk avoidance in the COLREGs. Centered on the target vessel, with its heading direction as the 0° reference, it divides the surrounding space into six sectors, A–F, based on the three basic encounter modes defined in the COLREGs [47–49]. As shown in Figure 2, areas I, II, and III represent the zones of head-on, crossing, and overtaking encounter patterns, respectively. Specifically, a head-on encounter is defined as approaching vessels between ±5° of direction F; a crossing encounter occurs between ±(5° and 112.5°) in directions A, B, and E; and an overtaking encounter occurs when the incoming vessel appears behind the target vessel between 112.5° and 247.5° in directions C and D. During collision avoidance maneuvers, the target vessel generally has the right of way and should maintain its course and speed when encountering vessels from sectors C, D, and E. Conversely, the target vessel is typically required to give way to vessels approaching from directions A, B, and F, maneuvering to starboard for vessels in sectors A and F and to port for vessels in sector B.

To effectively model the influence of surrounding vessels on the target vessel's trajectory, this study introduces VIM. This map divides the sea space around the target vessel into distinct zones based on encounter type and distance, as detailed in Table 1. The table shows the distance thresholds D_r for the three encounter modes (head-on, crossing, and overtaking), derived from the COLREGs and general operating habits of navigators. These thresholds are typically set as D_1 (6–8 nautical miles), D_2 (4–6 nautical miles), and D_3 (2–4 nautical miles) [1]. Accordingly, the VIM is divided into 12 zones (Figure 3) categorized by their distance from the central vessel: zones 1–6 cover 0–2 nautical miles; zones 7, 8, and 11 cover 2–6 nautical miles; zones 9 and 10 cover 2–4 nautical miles; and zone 12 covers 2–8 nautical miles. At each time step, a tensor of length 12 is constructed to represent the VIM. Each element of this tensor corresponds to one of the 12 zones and quantifies the impact of vessels in that zone on the target vessel—for instance as follows:

$$VIM_t = [S_{t,1}, \ldots, S_{t,i}, \ldots, S_{t,12}] \tag{15}$$

where $S_{t,i}$ represents the set of vessels in zone i at time t. Because the number of vessels in each zone is uncertain, we perform a mean pooling operation on each tensor element and

append the number of vessels as a feature. If no vessel exists in a zone, its tensor element is set as a zero vector. The feature vector $A_{t,i}$ of $S_{t,i}$ is specifically defined as

$$N_{t,i} = Count(S_{t,i})$$
$$A_{t,i} = \begin{cases} [\frac{1}{N_{t,i}} \sum_{k=1}^{N_{t,i}} O_{t,i,k}, N_{t,i}] & \text{if } N_{t,i} > 0, \\ zeros(8) & \text{otherwise} \end{cases} \quad (16)$$

where $N_{t,i}$ represents the number of vessels in zone i at time t and $O_{t,i,k}$ denotes the influence factor vector of the kth vessel in zone i at time t (Equation (14)). The VIM at the final moment t is

$$VIM_t = [A_{t,1}, \ldots, A_{t,i}, \ldots, A_{t,12}] \quad (17)$$

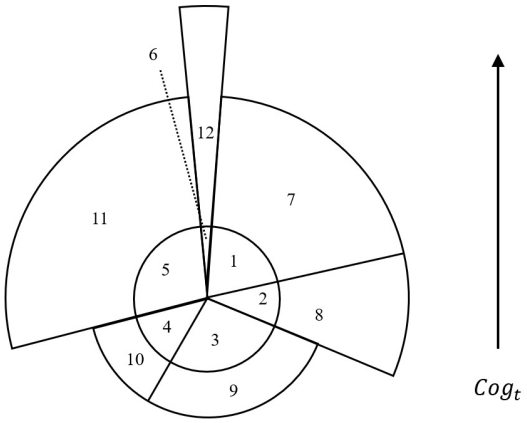


Figure 3. VIM. The numbers represent the zone numbers.

Table 1. Classification of encounter patterns.

	Head-On	**Crossing**	**Overtaking**
D_r	$D_r < D_1$	$D_r < D_2$	$D_r < D_3$
Course	(−5°, 5°)	(−112.5°, −5°) and (5°, 112.5°)	(112.5°, 247.5°)
Area	I	II	III

This process of standardizing the information of surrounding vessels around the target vessel is referred to as VIM pooling. Through this standardized description, VIM_t provides consistent input features in the face of uncertain numbers of surrounding vessels.

3.4. VI-LSTM

VI-LSTM consists of two main components: an encoder and a decoder (Figure 1). The encoder receives time-series data, including vessel motion factors, maritime environmental factors, and information regarding surrounding vessels. It extracts features through a specially designed feature extraction layer (FEL) and a BiLSTM network to generate a high-dimensional latent feature representation. The decoder introduces an attention mechanism to generate the contextual information that is the most relevant to the prediction moment and progressively predicts the future trajectory through an LSTM network. In addition, a temporally weighted hybrid loss function is specifically designed for the peculiarities of vessel trajectory prediction.

3.4.1. Encoder Network

The goal of the encoder is to understand and abstract the input time-series data $x_t = [P_t, E_t, VIM_t]$. For this purpose, we designed the FEL (Figure 4). The main task of this

layer is to extract the high-dimensional feature representations e_t from the original input at each moment:

$$e_t = \mathrm{FEL}(x_t) \tag{18}$$

where FEL is the feature extraction layer, x_t is the input data time t, and e_t is the high-dimensional feature description of the corresponding moment. The FEL consists of two main parts.

- First, the FEL concatenates the motion factors P_t and environmental factors E_t of the vessel and extracts the features through a fully connected (FC) layer to capture the interactions between the motion and environment.
- Second, the FEL employs three consecutive convolutional layers and an FC layer to extract features from the VIM_t, thereby capturing the influence of surrounding vessels on the future behavior of the target vessel.

The outputs of these two parts are subsequently merged into a feature vector, which serves as the input to the BiLSTM for subsequent trajectory prediction. The FEL shares parameters across different times to ensure consistency and efficiency.

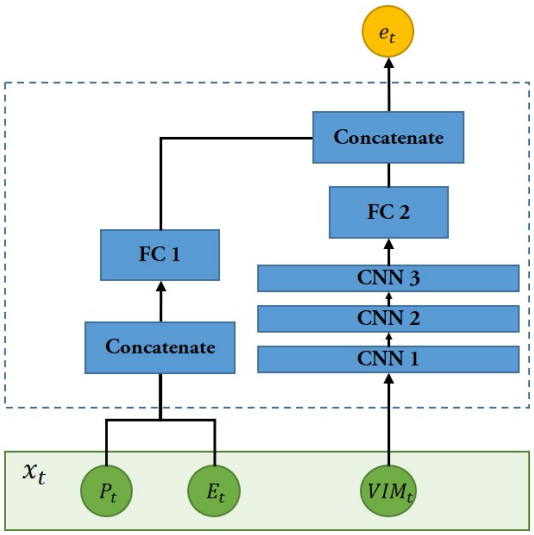


Figure 4. Feature extraction layer (FEL) network structure.

The encoder network employs a BiLSTM model [50] to capture the forward and backward temporal dependencies within the time-series data in both time directions. Each direction of the BiLSTM has independent weight matrices $\{\overrightarrow{W_E}, \overleftarrow{W_E}\}$ that allow it to learn the forward and backward temporal dependencies independently. The forward and backward hidden states at each moment are concatenated to form the final hidden state:

$$\overleftrightarrow{h_t} = [\overrightarrow{h_t}, \overleftarrow{h_t}] \tag{19}$$

The sequence of hidden states from the BiLSTM $H = [\overleftrightarrow{h_1}, \overleftrightarrow{h_2}, \ldots, \overleftrightarrow{h_T}]$ serves as the encoder output, providing a basis for generating contextual information for the subsequent attention mechanisms.

3.4.2. Decoder Network

For the prediction moment $t+1$, we compute the position description p_t as a decoder input based on the positions at times t and $t-1$:

$$\begin{aligned} \Delta lon_t &= lon_t - lon_{t-1} \\ \Delta lat_t &= lat_t - lat_{t-1} \\ p_t &= [lon_t, lat_t, \Delta lon_t, \Delta lat_t] \end{aligned} \tag{20}$$

We employ the additive attention mechanism (Bahdanau attention [51]) as an intermediary layer to facilitate information transfer between the encoder and decoder. The mechanism generates context information z_t, which is the most relevant to the current prediction, based on the position description p_t at time t:

$$z_t = \text{Attention}(p_t) \tag{21}$$

The decoder network employs LSTM to calculate the future positions of vessels iteratively:

$$S_{t+1}, o_{t+1} = \text{LSTM}([z_t, p_t], s_t) \tag{22}$$

where $[z_t, p_t]$ represents the feature vector formed by concatenating the context information z_t and position description p_t at moment t. The LSTM calculates the hidden state s_{t+1} and output features o_{t+1} for the next moment based on this vector and the current hidden state s_t.

Subsequently, we map the output feature o_{t+1} of the decoder LSTM to a five-dimensional vector using an FC layer, forming the prediction described in Equation (4).

In the process of initializing the hidden state of the decoder, we use both the static factors I and last hidden state of the forward LSTM in the encoder $\overrightarrow{h_T}$ as inputs (Figure 5). We concatenate the length and width and extract features through an FC layer. We textually index the vessel type and MMSI and convert the indexed values into feature vectors using an embedding layer. Subsequently, we merge these three feature vectors with $\overrightarrow{h_T}$ and regularize them through an FC layer to match the dimensionality of the hidden layers of the decoder.

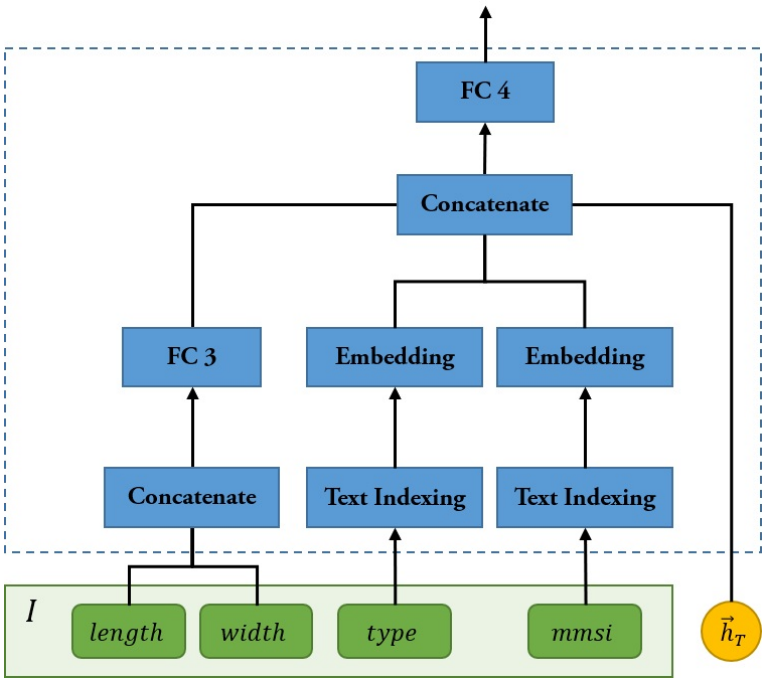


Figure 5. Decoder hidden state initialization network structure.

3.4.3. Loss Function

The loss function is crucial in deep learning, as it directly affects the model performance and training effectiveness. We consider three aspects for predicting trajectories: accuracy, uncertainty, and the importance of predictions at different moments. We propose a temporally weighted hybrid loss function to evaluate the practical performance of the model predictions comprehensively.

We use the Haversine formula to calculate the geographical distance between the predicted and actual positions to evaluate the accuracy of the position predictions. The prediction distance error $distance_t$ at time t is

$$\begin{aligned} \Delta lon &= lon_t - \mu_{lon,t} \\ \Delta lat &= lat_t - \mu_{lat,t} \\ a_t &= \sin^2\left(\frac{\Delta lat}{2}\right) + \cos\left(\mu_{lat,t}\right) \cdot \cos\left(lat_t\right) \cdot \sin^2\left(\frac{\Delta lon}{2}\right) \\ distance_t &= 2 \cdot R_E \cdot \arcsin\left(\sqrt{a_t}\right) \end{aligned} \tag{23}$$

where R_E is the radius of the earth, lon_t and lat_t are the actual positions of the vessel, and $\mu_{lon,t}$ and $\mu_{lat,t}$ are the predicted positions of the vessel.

We use the negative log-likelihood to evaluate the accuracy of the predicted positions and reliability of the uncertainty estimates. The negative log-likelihood is calculated as

$$nll_t = \frac{1}{2}(p_t - \hat{\mu}_t)^\top \hat{\Sigma}_t^{-1}(p_t - \hat{\mu}_t) + \frac{1}{2}\ln|\hat{\Sigma}_t| + \frac{D}{2}\ln 2\pi \tag{24}$$

where nll_t is the negative log-likelihood calculation of the predicted result at time t; $p_t = [lon_t, lat_t]$ is the actual position of the vessel; $\hat{\mu}_t$ and $\hat{\Sigma}_t$ are the mean and covariance matrix of the predicted position (Equation (5)), respectively; and D is the dimension of the predicted outcome, which is 2 in this case.

For the loss value at time t, we combine the two aforementioned evaluation methods via a weighted summation:

$$l_t = distance_t + \alpha \cdot nll_t \tag{25}$$

where α is the weight that balances the distance and negative log-likelihood.

The future trajectory is calculated iteratively based on the prediction of the previous moment. Thus, the accuracy of the previous step significantly affects the accuracy of the subsequent prediction. Therefore, we set different weights at different moments to guide the model to provide better trajectory predictions. The overall loss function is

$$loss = \sum_{t=T+1}^{H} w_t \cdot l_t \tag{26}$$

3.4.4. Implementation Details

We implemented the proposed model using the TensorFlow framework [52] and trained it on a personal computer equipped with an Intel Core i9-13900 processor, an NVIDIA GeForce RTX 3060Ti graphics card, and 32 GB DDR4 3200 memory. The backbone of the model comprises a BiLSTM encoder layer and an LSTM decoder layer, each of which has 96 hidden units (Figure 1). In Figures 4 and 5, the fully connected (FC) layers FC1, FC2, FC3, and FC4 have dimensions of 32, 32, 8, and 96, respectively. The convolutional neural network (CNN) layers CNN1, CNN2, and CNN3 have kernel sizes and channel numbers of (5 × 5, 16), (5 × 5, 24), and (3 × 3, 32), respectively. To prevent overfitting, both the LSTM structures and FC layers in the model employ L2 regularization with the regularization coefficient set to 0.1.

The training employs the Adam optimizer to adaptively adjust the learning rate, a batch size of 8, and 200 training epochs. The weight parameter α in the loss function (Equation (25)) is set to 12. We utilize a dynamic teacher forcing strategy to mitigate instability during training [53], starting with a probability of 1 and gradually decreasing to 0 by the 140th epoch.

A dropout mechanism is integrated into the BiLSTM and LSTM structure to capture the predictive uncertainty of the model, thereby enabling approximate variational inference [54]. During the processing of the same time series, the mask m_h is synchronously applied at each moment to maintain the coherence of the information flow within the LSTM cells throughout the time series. In the prediction phase, we use the Monte Carlo (MC) dropout method to estimate the epistemic uncertainty of the model [55]. The dropout rate is set to 0.05, and the number of predictions for Monte Carlo (MC) dropout is 100.

4. Experimental Results and Analysis

4.1. Data Description

In this study, we used automatic identification system data[2] from 2019, published by the National Oceanic and Atmospheric Administration of the United States. The experimental area was the Galveston Bay area, specifically within the longitudinal range from −95.3027° to −93.9050° and the latitudinal range from 28.8783° to 29.9825°. This region covers the Houston Ship Channel, Texas City, Galveston Bay, and its southeastern waters. It is one of the major oil export ports and the largest estuary in the US, and it plays a crucial role in trade and transportation activities in the southern United States. In addition, it is characterized by complex maritime traffic patterns.

We obtained 9154 vessel trajectories from 910 distinct vessels within the experimental area, generating 25,884 prediction samples. These data encompass nine different vessel types, including tankers, towing vessels, cargoes, fishing vessels, pleasure craft, sailing vessels, passenger vessels, local vessels, and tugboats. Figure 6 depicts the geographical locations and trajectory distribution of the experimental data. The blue rectangle marks the data coverage area and the heatmap shows the density of the trajectory distribution, with the red and blue areas indicating high and low density, respectively.

We employed the data processing methods described in [56], which include denoising, removing stationary trajectories from the raw data, and standardizing the original trajectories to 5 min intervals. Each sample includes historical time-series information X for the 2 h preceding the prediction moment, the static information of the vessel I, and the actual trajectory Y for 1 h following the prediction moment. We optimized the MySQL database by setting time, lon, and lat indices to enhance the efficiency of querying the surrounding vessel information.

To evaluate both the training performance and the generalization ability of the proposed model, the dataset was partitioned into three subsets: training, test, and unseen subject test. To ensure a robust evaluation of generalization ability, the unseen subject test set was constructed by randomly selecting 10 vessels representing a diverse range of vessel types, sizes, and operational characteristics. This diversity is crucial for assessing the model's performance on vessels with potentially different maneuvering patterns and responses to environmental conditions. This selection included two tankers, two towing vessels, two cargo vessels, one fishing vessel, one pleasure craft, one sailing vessel, and one passenger vessel. Local vessels and tugboats were excluded from this selection owing to their limited number and relatively simple behavior patterns constraints within a confined area. In contrast, tankers, towing vessels, and cargo vessels are more numerous and play a crucial role in maritime transportation, making their accurate trajectory prediction particularly important to maritime monitoring.

The samples generated by these 10 vessels were exclusively used to evaluate the generalization ability of the model to unknown vessels and were not involved in the training process. The remaining samples were randomly assigned to the training and test sets at a ratio of 8:2. This ratio was selected to provide sufficient data for training while reserving an adequate portion for evaluating the model's performance on known vessel

types. The resulting numbers of samples in the training, test, and unseen subject test sets were 20,480, 5121, and 283, respectively.

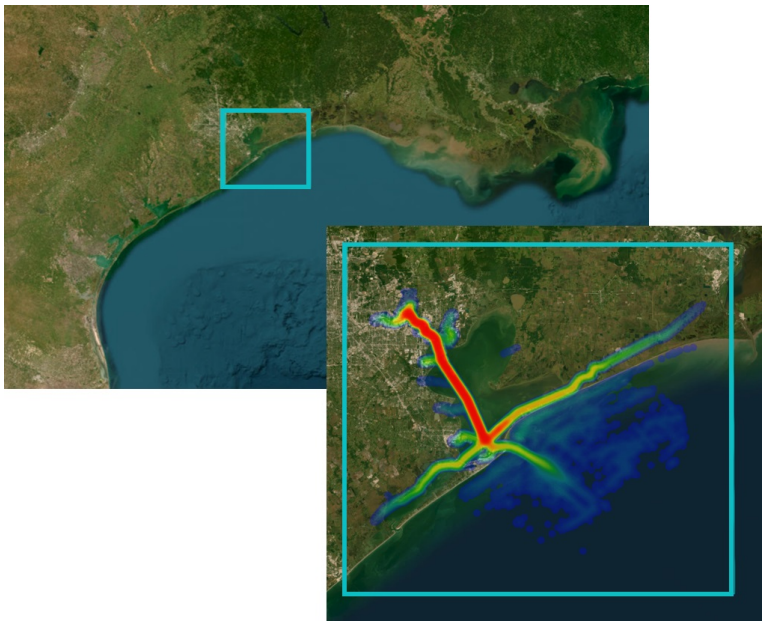


Figure 6. Geographical location and trajectory distribution of the experimental data. The blue rectangle marks the data coverage area and the heatmap shows the density of the trajectory distribution, with the red and blue areas indicating high and low density, respectively.

4.2. Performance Evaluation

Figure 7 shows the prediction results obtained by the VI-LSTM, where the blue line represents the historical trajectory of the vessel for 2 h before the prediction moment, the green line indicates the actual future trajectory over the next 1 h, and the orange line shows the predicted future trajectory. The orange elliptical areas centered on the points represent confidence ranges of 0.25, 0.50, and 0.75 for the prediction. The image on the right displays a magnified view of the predicted segment of the trajectory.

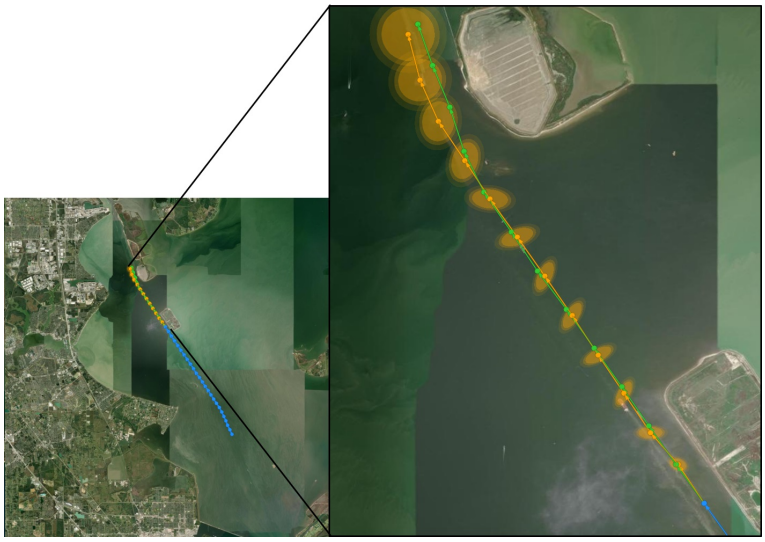


Figure 7. Illustration of sample prediction results. The left image shows the complete trajectory sample along with its predicted results. The blue line represents the vessel's historical trajectory for the 2 h preceding the prediction time, while the green line indicates the actual future trajectory for the next hour. The orange line represents the predicted trajectory, and the orange elliptical region depicts the confidence range of the prediction at each time step. The right image provides a magnified view of the predicted segment of the trajectory.

We considered several performance evaluation metrics to evaluate the predictive performance of the model comprehensively.

4.2.1. Mean Haversine Distance Error (MDE)

The Haversine distance is used to calculate the distance between two points on a sphere. The calculation process is shown in Equation (23). We calculated the mean distance between the actual and predicted points to obtain the MDE of the sample, which intuitively assessed how closely the trajectory predicted by the model aligned with the actual trajectory. The calculation formula is

$$MDE = \frac{1}{N}\sum_{t=1}^{N} Hav(\hat{y}_t, y_t) \tag{27}$$

where N represents the number of prediction moments and $Hav(\hat{y}_t, y_t)$ represents the Haversine distance between the predicted position $\hat{y}_t$ and actual position y_t at time t.

4.2.2. Root Mean Square Error (RMSE)

The RMSE between the predicted and actual values is sensitive to outliers and can reflect the degree of deviation of the predicted values from the actual values. The calculation formula is

$$RMSE = \sqrt{\frac{1}{N}\sum_{t=1}^{N}\left(\left(\hat{lon}_t - lon_t\right)^2 + \left(\hat{lat}_t - lat_t\right)^2\right)} \tag{28}$$

4.2.3. Mean Absolute Error (MAE)

The MAE between the predicted and actual values is less sensitive to outliers than the $RMSE$ and it better reflects the overall deviation of the predicted values. The calculation formula is

$$MAE = \frac{1}{N}\sum_{t=1}^{N}\left(\left|\hat{lon}_t - lon_t\right| + \left|\hat{lat}_t - lat_t\right|\right) \tag{29}$$

4.2.4. Accuracy (ACC)

Accuracy is used to evaluate the accuracy of the confidence ranges of the model by measuring whether the predicted confidence ranges contain the actual points. The calculation formula is

$$\begin{aligned} n &= \sum_{t=1}^{N}\begin{cases} 0 & \text{if in the confidence ellipse,} \\ 1 & \text{else} \end{cases} \\ ACC &= \frac{n}{N} \end{aligned} \tag{30}$$

where n is the number of moments in which the actual trajectory points fall within the predicted confidence ranges. The accuracy for the three confidence ranges was calculated independently, and in the subsequent sections, ACC_{25}, ACC_{50}, and ACC_{75} represent the accuracy of the confidence ranges at confidence levels of 0.25, 0.5, and 0.75, respectively.

4.3. Comparative Experiment

This section provides a comparative analysis of the predictive capabilities of various deep learning methods. The hyperparameters of the tested models were meticulously selected through an extensive optimization process. The following models were used for comparison:

1. LSTM [57]. This method utilizes a multilayer recurrent neural network to extract high-dimensional features from the input data and then predicts the position of the vessel at future time points through LSTM layers.
2. BiLSTM [29]. This method employs BiLSTM layers to capture bidirectional features of the time-series data. Subsequently, it merges the hidden states at each time point and predicts the future position of the vessel through an FC layer.
3. BiLSTM-LSTM [33]. This method adopts an encoder–decoder architecture in which the encoder is composed of BiLSTM and the decoder is composed of LSTM. Context information for the current prediction is generated by integrating the position information from the previous moment and hidden states of the encoder using an attention mechanism. Subsequently, the decoder iteratively predicts the future trajectory of the vessel.
4. Transformer [58]. This method employs a classic Transformer encoder–decoder architecture. Each encoder block contains multi-head self-attention mechanisms and feed-forward networks that are enhanced by residual connections and layer normalization techniques to stabilize the training process. The decoder block adds a masked multi-head self-attention mechanism based on the encoder block, and both the encoder and decoder are composed of multiple such stacked blocks.
5. TRFM-LSTM [39]. This method refines each encoder block of the Transformer by adding an independent LSTM layer to extract temporal dependencies in the sequence. The LSTM layer output is fused with the original encoder block output to form the final output of the encoder block.

Table 2 presents the performance evaluation results of the aforementioned models on the two test sets. The table includes two columns for percentage improvement (IMP), which show the improved performance of VI-LSTM compared to each comparative model on the test sets. The IMP is calculated as the average of the percentage improvements across three evaluation metrics: MDE, RMSE, and MAE. For each metric, the IMP_{mec} is computed as

$$IMP_{Mec} = \frac{Mec_{model} - Mec_{VI-LSTM}}{Mec_{model}} \times 100\% \tag{31}$$

where Mec_{model} and $Mec_{VI-LSTM}$ represent the performances of the comparative and proposed model, respectively, based on Mec's evaluation method. The IMP values further highlight the significant improvement of the VI-LSTM method across all evaluation metrics, with improvements ranging from 56.63% to 67.15% compared to the comparative models, thereby indicating substantial improvement in the vessel trajectory prediction accuracy.

Table 2. Predictive performance evaluation of comparative methods.

	Test Set				Unseen Subject Test Set			
Model	**MDE (m)**	**RMSE (°)**	**MAE (°)**	**IMP**	**MDE (m)**	**RMSE (°)**	**MAE (°)**	**IMP**
VI-LSTM	330.6556	0.00388	0.00412	-	480.2992	0.00540	0.00593	-
LSTM	848.3428	0.00998	0.01057	61.06%	1273.8999	0.01485	0.01582	62.82%
BiLSTM	765.4708	0.00919	0.00955	57.15%	1152.5029	0.01363	0.01433	59.11%
BiLSTM-LSTM	758.2861	0.00905	0.00944	56.63%	1123.1224	0.01313	0.01388	57.79%
Transformer	972.6877	0.01131	0.01204	65.83%	1238.1354	0.01450	0.01533	61.76%
TRFM-LSTM	1015.9440	0.01170	0.01254	67.15%	1294.7007	0.01494	0.01601	63.24%

Figure 8 shows the box plot of the MDE for each method. Compared with the other methods, VI-LSTM exhibited noticeably lower and more concentrated distance errors, highlighting its distinct advantages in prediction accuracy and stability. In addition, on the

test set, the low-end whiskers of all methods were relatively close; however, the high-end whisker of VI-LSTM was markedly lower than those of the other methods. Thus, although all methods performed well with simple samples, VI-LSTM demonstrated a clear advantage in handling complex samples. On the unseen subject test set, only the low-end whisker of VI-LSTM was close to its performance on the test set, with the other methods showing noticeable increases.

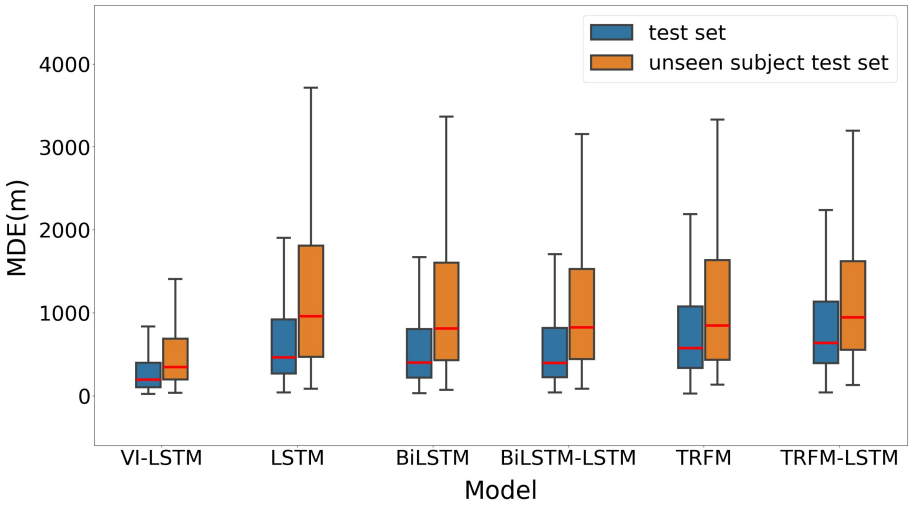


Figure 8. Comparison of MDEs predicted by different methods. The box plot in the figure illustrates the range from the first quartile to the third quartile, with the red horizontal line representing the median.

Figures 9–11 visualize the predicted trajectories for three samples of varying difficulties, representing the first quartile, median, and third quartile of distance errors for VI-LSTM on the test set. These examples illustrate the model's performance in scenarios with near-linear movement, abrupt turns, and continuous course changes, providing a comprehensive overview of its capabilities across different conditions.

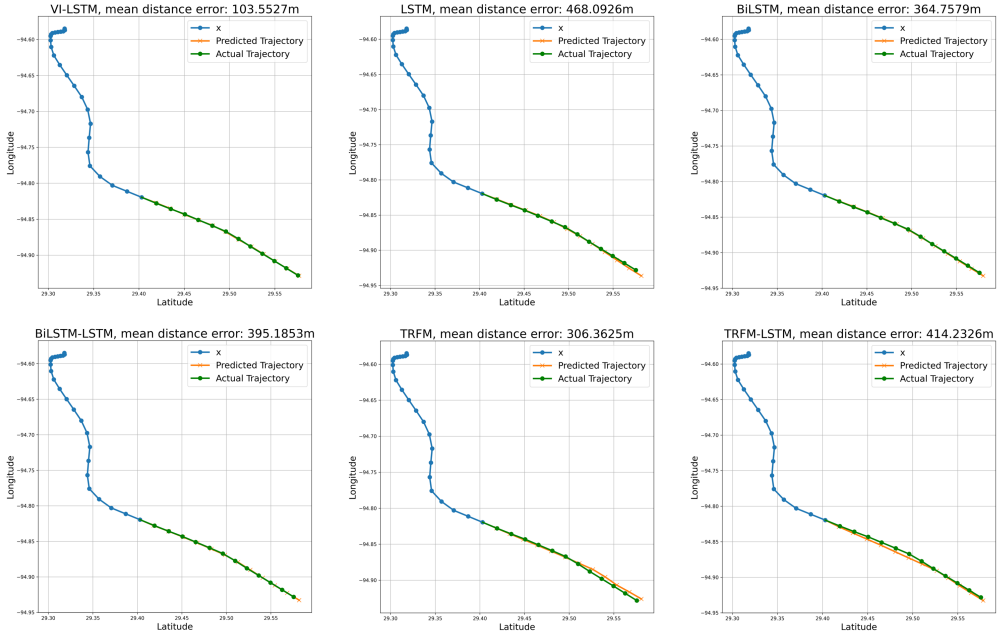


Figure 9. Tanker vessel. MMSI 356,899,000; length: 183 m; width: 32 m; predicted moment: 2019-01-17T22:38:52; time state: dawn or dusk; average number of surrounding vessels: 47.92.

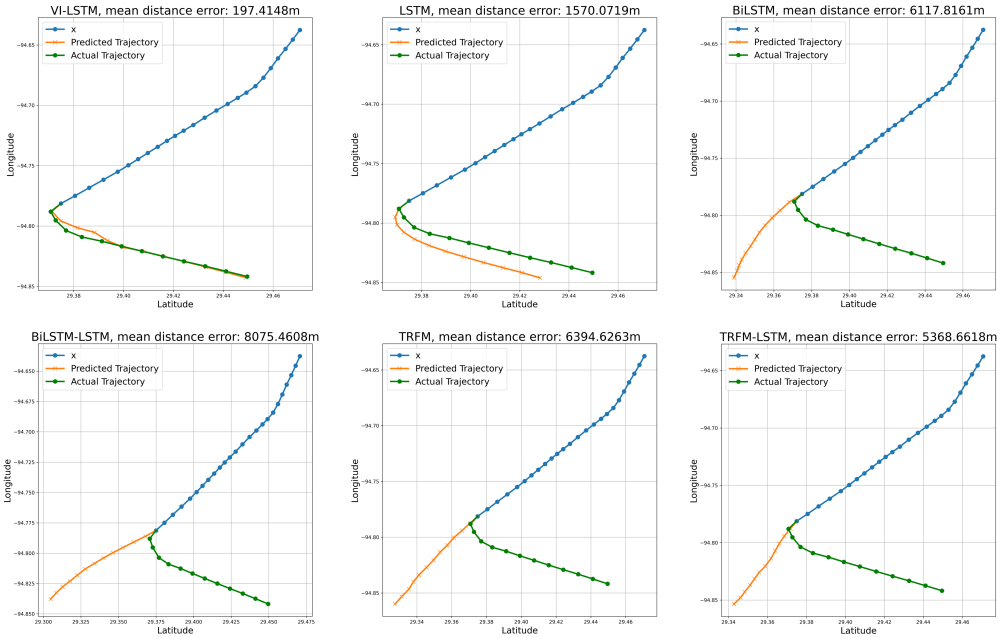


Figure 10. Towing vessel. MMSI: 367,095,660; length: 22 m; width: 7 m; predicted moment: 2019-05-07T06:35:15; time state: night; average number of surrounding vessels: 24.4.

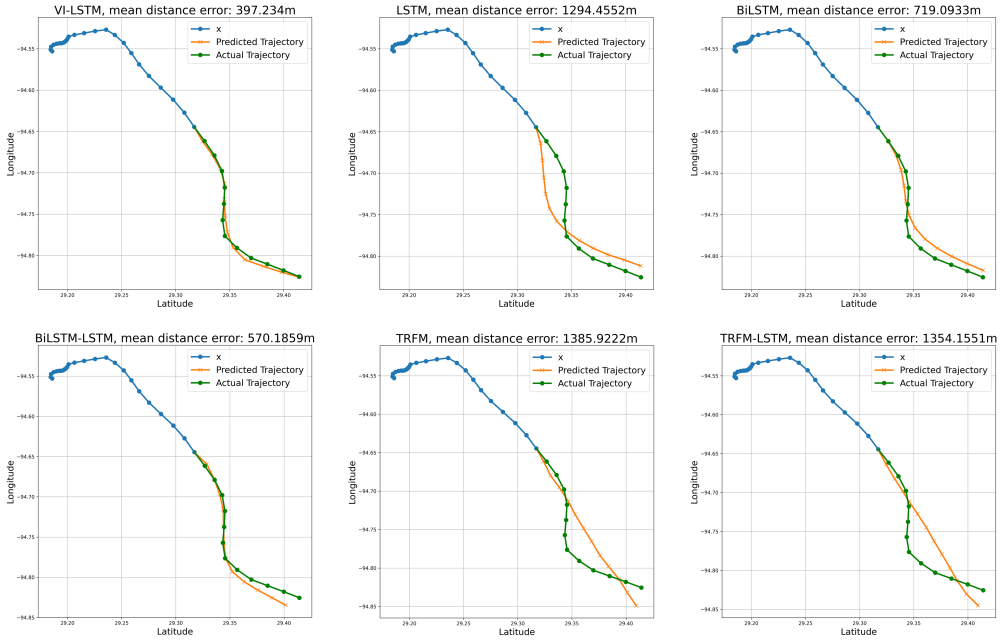


Figure 11. Tanker vessel. MMSI: 240,435,000; length: 243 m; width: 42 m; predicted moment: 2019-08-22T12:20:14; time state: dawn or dusk; average number of surrounding vessels: 36.92.

Figure 9 illustrates a scenario where a vessel maintains a steady course and speed without significant environmental disturbances, resulting in a near-linear trajectory. The target vessel, observed at dusk or dawn, had approximately 48 surrounding vessels recorded over the preceding two hours. For this sample, all models performed well in predicting the vessel's future position. However, VI-LSTM achieved a remarkably low MDE of approximately 104 m, whereas the MDE of all other methods exceeded 300 m. By leveraging the VIM, VI-LSTM effectively captured subtle environmental effects on the target vessel, enhancing the prediction accuracy even in this near-linear sailing scenario. This result indicates that VI-LSTM not only demonstrates notable advantages in complex environments but also provides highly accurate predictions under relatively simple conditions. Figure 10

illustrates a challenging scenario where a vessel makes an abrupt turn shortly after the prediction moment, as often happens when entering a port or navigating around obstacles. In this example, the target vessel, observed at night with approximately 24 surrounding vessels tracked over the preceding two hours, maintained a near-linear trajectory before suddenly changing heading. This requires models to quickly capture and respond to the shift. The results show that only VI-LSTM and LSTM successfully identified this turn. However, while LSTM predicted the correct turning direction, its estimation of the turning path was less accurate, resulting in an MDE exceeding 1500 m. The other models failed to detect the turn, yielding MDE values over 5000 m. In contrast, VI-LSTM achieved an MDE of less than 200 m. This superior performance is attributed to VI-LSTM's ability to integrate temporal and spatial features, accurately modeling pre- and post-turn dynamics and sustaining high accuracy and stability even in rapid turning scenarios. This highlights the robustness of VI-LSTM in highly dynamic conditions.

Figure 11 presents a challenging scenario where a vessel continuously changes course, a behavior commonly observed during complex maneuvers or when navigating intricate routes. The unpredictable timing, angle, and radius of these turns make accurate prediction particularly difficult. In this example, the target vessel, observed at dusk or dawn with approximately 37 surrounding vessels recorded over the preceding two hours, continuously altered its course, following a curved trajectory. This presents additional challenges for models attempting to capture these complex motion patterns. The results show that LSTM, Transformer, and TRFM-LSTM struggled to predict the vessel's future trajectory, each exhibiting an MDE greater than 1000 m. In contrast, VI-LSTM, BiLSTM, and BiLSTM-LSTM provided better results, suggesting that BiLSTM-based architectures are more effective at capturing the intricate temporal dependencies inherent in continuous turning scenarios. However, BiLSTM-LSTM and LSTM suffered from cumulative error and memory decay over prolonged turning sequences, leading to increased errors later in the prediction. By leveraging a specially designed time-weighted mixed loss function, VI-LSTM effectively learned complex, long-duration motion patterns, significantly improving prediction performance in this challenging scenario.

Collectively, these three prediction examples illustrate the notable advantages of VI-LSTM across diverse navigational scenarios. Whether the vessel followed a simple near-linear route or underwent abrupt and sustained turning maneuvers, VI-LSTM consistently achieved more accurate and stable forecasts, demonstrating robust generalization capabilities. Compared with the other models, VI-LSTM not only exhibited considerably lower average errors but also showed a more concentrated and stable error distribution, particularly under extreme or complex conditions, which is an essential attribute for practical applications. Furthermore, VI-LSTM continued to perform at a high level on the unseen subject test set, providing further evidence of its adaptability to varying data distributions and novel vessel behaviors. Consequently, VI-LSTM can reliably predict trajectories even in previously unobserved circumstances, underscoring its potential for real-world deployment.

In contrast, Transformer-based models, despite their advanced multi-head attention mechanisms and positional encoding that can capture complex temporal dependencies, underperformed in this study. This is attributed to two main factors. First, vessel trajectory prediction inherently relies on temporal continuity, with future behaviors strongly influenced by past motion inertia—something LSTM and Bi-LSTM are better suited for. Second, the limited size and information density of the dataset in this study may have hindered the effectiveness of Transformer models, which typically thrive on large-scale, diverse data. However, with larger, more comprehensive datasets, Transformers could offer advantages in processing multi-modal data (e.g., weather, charts, events) and building

large-scale predictive models. Integrating Transformers with traditional sequential models to better address complex trajectory prediction tasks remains a promising avenue for future research.

4.4. Ablation Experiment

This section describes an ablation experiment that was conducted to evaluate the effects of individual components on the overall performance by systematically removing key elements from our model. The specific experimental setups were as follows.

1. Baseline model. The complete model, including all designed components, served as the benchmark for comparison.
2. Variant 1. The static information I was not utilized, that is, $\overrightarrow{h_T}$ from Figure 5 was directly fed into FC 4 to initialize the hidden state of the decoder.
3. Variant 2. The environmental information E_t was not utilized, that is, P_t from Figure 4 was directly input into FC 1.
4. Variant 3. The vessel influence factors were excluded; specifically, the three-dimensional features $DPCA_{t,k}, TPCA_{t,k}, and\ ST_{t,k}$ were removed, as outlined in Equation (14).
5. Variant 4. The influence information of the surrounding vessels VIM_t was not employed, with the output of FC 1 from Figure 4 serving as the final output of this architecture.
6. Variant 5. The loss function utilized only the distance error, expressed as in Equation (25), adjusted to $l_t = distance_t$.
7. Variant 6. The loss function employed solely the logarithmic likelihood error, expressed as in Equation (25), adjusted to $l_t = nll_t$.
8. Variant 7. Equal weighting was applied across different times in the loss function, with each time point t weight in Equation (26) set to $w_t = \frac{1}{H-T}$.

Table 3 presents the performance evaluation results of each variant on the two test datasets. The baseline model performed optimally across three performance indicators on both datasets. Excluding the baseline, variant 5 exhibited the best performance, with an increase of only approximately 0.4% in the MDE, suggesting that the negative logarithmic likelihood loss function had a minimal effect on the prediction accuracy. However, Table 4 demonstrates that the absence of the negative logarithmic likelihood error in the loss function of variant 5 significantly reduced the accuracy of the confidence ranges, which demonstrates the critical importance of the negative logarithmic likelihood loss in the accuracy of uncertainty estimations. Variant 6 exhibited the poorest performance, with errors that were approximately 90% higher than those of the baseline model, underscoring the vital role of the distance error loss function in ensuring the accuracy of the predictive model. The performance losses of other variants ranged from 1% to 5%, indicating that the static information, environmental data, vessel influence features, VIM, and temporal weighting in the loss function all enhance the accuracy of the predictive model.

Because the vessels in the unseen subject test set were not part of the model training, the prediction difficulty for these samples was more serious, resulting in a loss of approximately 45% in the prediction performance for the baseline model within this dataset. Moreover, variants 3 and 4 exhibited considerable losses in performance of approximately 51% and 60%, respectively. These losses occurred primarily because of the absence of vessel influence factors and VIM_t. Hence, these results illustrate the importance of quantifying the influence of surrounding vessels.

Table 3. Comparison of overall prediction performance between the variant models and baseline model.

Model	Test Set			Unseen Subject Test Set		
	MDE (m)	RMSE (°)	MAE (°)	MDE (m)	RMSE (°)	MAE (°)
Baseline model	330.6556	0.00388	0.00412	480.2992	0.00540	0.00593
Variant 1	346.8548	0.00409	0.00433	507.7029	0.00571	0.00632
Variant 2	340.8036	0.00396	0.00425	487.1029	0.00549	0.00601
Variant 3	336.2781	0.00394	0.00419	508.6785	0.00574	0.00633
Variant 4	335.0766	0.00393	0.00417	535.8102	0.00611	0.00665
Variant 5	332.1013	0.00393	0.00415	483.6687	0.00547	0.00599
Variant 6	626.6349	0.00659	0.00781	1154.719	0.01167	0.01412
Variant 7	338.8257	0.00395	0.00422	484.9425	0.00548	0.00602

Table 4. Confidence range accuracies of the variant models compared with that of the baseline model.

Model	ACC_{25}	ACC_{50}	ACC_{75}
Baseline model	73.83%	80.08%	86.69%
Variant 1	75.23%	81.44%	87.09%
Variant 2	68.30%	76.49%	84.16%
Variant 3	71.79%	78.98%	85.40%
Variant 4	73.16%	80.14%	86.38%
Variant 5	12.52%	16.98%	23.48%
Variant 6	70.26%	81.69%	89.52%
Variant 7	73.37%	80.30%	86.28%

5. Conclusions

This study has proposed the innovative VI-LSTM model that significantly enhances the accuracy and reliability of vessel trajectory prediction. We systematically identified and categorized the key factors affecting future vessel trajectories into vessel motion, environmental, vessel static, and vessel influence factors. Our model effectively quantifies the effects of surrounding vessels on the target vessel by introducing the VIM structure, thereby improving the predictive accuracy and generalization capabilities of the model. Furthermore, it predicts the future position of a vessel as a Gaussian distribution and includes an MC dropout technique to estimate the uncertainty of the prediction results, which enhances the practicality and interpretability of the model. A temporally weighted hybrid loss function further enhances the fitting capability of the model.

In comparative and ablation experiments conducted with real maritime trajectory data, VI-LSTM achieved an MDE of merely 330.66 m for predicting vessel trajectories over the next hour and 480.30 m on an unseen subject test set, significantly outperforming other deep learning methods across several evaluation metrics. Ablation experiments further validated the significant contributions of the VIM, loss function, and key factors to the predictive performance of the model. Our research demonstrates that the proposed model and methodologies provide crucial technical support and a theoretical basis for future research and applications in vessel trajectory prediction.

While this study demonstrates significant advancements in vessel trajectory prediction, we acknowledge certain limitations. First, our experiments primarily focused on the Galveston Bay area, which may not fully represent the diverse conditions of other maritime regions. Second, the computational scalability of our model with larger datasets requires further investigation. Future work will involve expanding the dataset to encompass more

varied maritime environments and vessel behaviors, enabling a deeper exploration of the factors influencing vessel behavior and an assessment of our model's adaptability to more complex scenarios. Our long-term goal is to develop an online system for predicting vessel behavior to enhance maritime situation monitoring. To ensure scalability for such applications, we will explore strategies such as model optimization, algorithm acceleration, and distributed training.

Author Contributions: Conceptualization, Z.G. and X.P.; methodology, Z.G., H.Q. and X.P.; writing—original draft, Z.G.; writing—review and editing, Z.G.; formal analysis, Z.G. All authors have read and agreed to the published version of the manuscript.

Funding: This research received no external funding.

Institutional Review Board Statement: Not applicable.

Informed Consent Statement: Not applicable.

Data Availability Statement: All data used in this study are publicly available. AIS data were obtained from the National Oceanic and Atmospheric Administration of the United States (https://coast.noaa.gov/htdata/CMSP/AISDataHandler/2019/, accessed on 12 February 2025). Seawater depth data were sourced from the GEBCO Global Bathymetry Dataset (https://www.gebco.net/, accessed on 12 February 2025).

Conflicts of Interest: The authors declare no conflicts of interest.

Notes

[1] Seawater depth from GEBCO Global Bathymetry Dataset (https://www.gebco.net/, accessed on 12 February 2025).
[2] https://coast.noaa.gov/htdata/CMSP/AISDataHandler/2019/, accessed on 12 February 2025.

References

1. Jiang, P.; Fan, Z.; Pan, M.; Hu, W. Research of traffic flow saturation on waters of the coastal ship routing system. *Ocean Eng.* **2022**, *263*, 112417. [CrossRef]
2. Alizadeh, D.; Alesheikh, A.A.; Sharif, M. Prediction of vessels locations and maritime traffic using similarity measurement of trajectory. *Ann. GIS* **2021**, *27*, 151–162. [CrossRef]
3. Venskus, J.; Treigys, P.; Markevičiūtė, J. Unsupervised marine vessel trajectory prediction using LSTM network and wild bootstrapping techniques. *Nonlinear Anal. Model. Control* **2021**, *26*, 718–737. [CrossRef]
4. Hochreiter, S.; Schmidhuber, J. Long short-term memory. *Neural Comput.* **1997**, *9*, 1735–1780. [CrossRef]
5. Graves, A.; Schmidhuber, J. Framewise phoneme classification with bidirectional LSTM and other neural network architectures. *Neural Netw.* **2005**, *18*, 602–610. [CrossRef]
6. Zhang, X.; Fu, X.; Xiao, Z.; Xu, H.; Qin, Z. Vessel trajectory prediction in maritime transportation: Current approaches and beyond. *IEEE Trans. Intell. Transp. Syst.* **2022**, *23*, 19980–19998. [CrossRef]
7. Li, H.; Jiao, H.; Yang, Z. Ship trajectory prediction based on machine learning and deep learning: A systematic review and methods analysis. *Eng. Appl. Artif. Intell.* **2023**, *126*, 107062. [CrossRef]
8. Semerdjiev, E.; Mihaylova, L. Variable-and Fixed-Structure Augmented Interacting Multiple-Model Algorithms for Manoeuvring Ship Tracting Based on New Ship Models. *Int. J. Appl. Math. Comput. Sci.* **2000**, *10*, 591–604.
9. Last, P.; Bahlke, C.; Hering-Bertram, M.; Linsen, L. Comprehensive analysis of automatic identification system (AIS) data in regard to vessel movement prediction. *J. Navig.* **2014**, *67*, 791–809. [CrossRef]
10. Scheepens, R.; van de Wetering, H.; van Wijk, J.J. Contour based visualization of vessel movement predictions. *Int. J. Geogr. Inf. Sci.* **2014**, *28*, 891–909. [CrossRef]
11. Üney, M.; Millefiori, L.M.; Braca, P. Data driven vessel trajectory forecasting using stochastic generative models. In Proceedings of the ICASSP 2019—2019 IEEE International Conference on Acoustics, Speech and Signal Processing (ICASSP), Brighton, UK, 12–17 May 2019; IEEE: Piscataway, NJ, USA, 2019; pp. 8459–8463.
12. Guo, S.; Liu, C.; Guo, Z.; Feng, Y.; Hong, F.; Huang, H. Trajectory prediction for ocean vessels base on K-order multivariate Markov chain. In Proceedings of the Wireless Algorithms, Systems, and Applications: 13th International Conference, WASA 2018, Tianjin, China, 20–22 June 2018; Proceedings 13; Springer: Berlin/Heidelberg, Germany, 2018; pp. 140–150.

13. Burger, C.N.; Grobler, T.L.; Kleynhans, W. Discrete kalman filter and linear regression comparison for vessel coordinate prediction. In Proceedings of the 2020 21st IEEE International Conference on Mobile Data Management (MDM), Versailles, France, 30 June–3 July 2020; IEEE: Piscataway, NJ, USA, 2020; pp. 269–274.
14. Lian, Y.; Yang, L.; Lu, L.; Sun, J.; Lu, Y. Research on ship AIS trajectory estimation based on particle filter algorithm. In Proceedings of the 2019 11th International Conference on Intelligent Human-Machine Systems and Cybernetics (IHMSC), Hangzhou, China, 24–25 August 2019; IEEE: Piscataway, NJ, USA, 2019; Volume 1, pp. 305–308.
15. Liu, J.; Shi, G.; Zhu, K. Vessel trajectory prediction model based on AIS sensor data and adaptive chaos differential evolution support vector regression (ACDE-SVR). *Appl. Sci.* **2019**, *9*, 2983. [CrossRef]
16. Liu, X.; He, W.; Xie, J.; Chu, X. Predicting the trajectories of vessels using machine learning. In Proceedings of the 2020 5th International Conference on Control, Robotics and Cybernetics (CRC), Wuhan, China, 16–18 October 2020; IEEE: Piscataway, NJ, USA, 2020; pp. 66–70.
17. Zhang, Z.; Ni, G.; Xu, Y. Trajectory prediction based on AIS and BP neural network. In Proceedings of the 2020 IEEE 9th Joint International Information Technology and Artificial Intelligence Conference (ITAIC), Chongqing, China, 11–13 December 2020; IEEE: Piscataway, NJ, USA, 2020; Volume 9, pp. 601–605.
18. Mazzarella, F.; Arguedas, V.F.; Vespe, M. Knowledge-based vessel position prediction using historical AIS data. In Proceedings of the 2015 Sensor Data Fusion: Trends, Solutions, Applications (SDF), Bonn, Germany, 6–8 October 2015; IEEE: Piscataway, NJ, USA, 2015; pp. 1–6.
19. Gan, S.; Liang, S.; Li, K.; Deng, J.; Cheng, T. Ship trajectory prediction for intelligent traffic management using clustering and ANN. In Proceedings of the 2016 UKACC 11th International Conference on Control (CONTROL), Belfast, UK, 31 August–2 September 2016; IEEE: Piscataway, NJ, USA, 2016; pp. 1–6.
20. Pallotta, G.; Vespe, M.; Bryan, K. Vessel pattern knowledge discovery from AIS data: A framework for anomaly detection and route prediction. *Entropy* **2013**, *15*, 2218–2245. [CrossRef]
21. Park, J.; Jeong, J.; Park, Y. Ship trajectory prediction based on bi-LSTM using spectral-clustered AIS data. *J. Mar. Sci. Eng.* **2021**, *9*, 1037. [CrossRef]
22. Murray, B.; Perera, L.P. Ship behavior prediction via trajectory extraction-based clustering for maritime situation awareness. *J. Ocean Eng. Sci.* **2022**, *7*, 1–13. [CrossRef]
23. Jiang, J.; Zuo, Y. Prediction of ship trajectory in nearby port waters based on attention mechanism model. *Sustainability* **2023**, *15*, 7435. [CrossRef]
24. Dobrkovic, A.; Iacob, M.E.; van Hillegersberg, J. Maritime pattern extraction and route reconstruction from incomplete AIS data. *Int. J. Data Sci. Anal.* **2018**, *5*, 111–136. [CrossRef]
25. Arguedas, V.F.; Pallotta, G.; Vespe, M. Maritime traffic networks: From historical positioning data to unsupervised maritime traffic monitoring. *IEEE Trans. Intell. Transp. Syst.* **2017**, *19*, 722–732. [CrossRef]
26. Kim, K.I.; Lee, K.M. Deep learning-based caution area traffic prediction with automatic identification system sensor data. *Sensors* **2018**, *18*, 3172. [CrossRef]
27. Shin, Y.; Kim, N.; Lee, H.; In, S.Y.; Hansen, M.; Yoon, Y. Deep learning framework for vessel trajectory prediction using auxiliary tasks and convolutional networks. *Eng. Appl. Artif. Intell.* **2024**, *132*, 107936. [CrossRef]
28. Li, X.; Liu, C.; Li, J.; Zhao, L.; Du, Z. Advancing ship trajectory prediction: Integrating deep learning with enhanced reference trajectory correction techniques. *Ocean Eng.* **2024**, *311*, 118880. [CrossRef]
29. Yang, C.H.; Wu, C.H.; Shao, J.C.; Wang, Y.C.; Hsieh, C.M. AIS-based intelligent vessel trajectory prediction using bi-LSTM. *IEEE Access* **2022**, *10*, 24302–24315. [CrossRef]
30. Li, H.; Xing, W.; Jiao, H.; Yang, Z.; Li, Y. Deep bi-directional information-empowered ship trajectory prediction for maritime autonomous surface ships. *Transp. Res. Part E Logist. Transp. Rev.* **2024**, *181*, 103367. [CrossRef]
31. Chen, J.; Zhang, J.; Chen, H.; Zhao, Y.; Wang, H. A TDV attention-based BiGRU network for AIS-based vessel trajectory prediction. *Iscience* **2023**, *26*, 106383 . [CrossRef]
32. Yoo, S.L.; Lee, K.; Baek, W.K.; Kim, K.I. Path Prediction for Fishing Boats Using Attention-Based Bidirectional Gated Recurrent Unit. *Ocean Sci. J.* **2024**, *59*, 3. [CrossRef]
33. Capobianco, S.; Forti, N.; Millefiori, L.M.; Braca, P.; Willett, P. Recurrent encoder-decoder networks for vessel trajectory prediction with uncertainty estimation. *IEEE Trans. Aerosp. Electron. Syst.* **2022**, *59*, 2554–2565. [CrossRef]
34. Yang, X.; Han, Z.; Zhang, Y.; Liu, H.; Liu, S.; Ai, W.; Liu, J. VEPO-S2S: A VEssel Portrait Oriented Trajectory Prediction Model Based on S2S Framework. *Appl. Sci. (2076-3417)* **2024**, *14*, 6344. [CrossRef]
35. Wang, S.; He, Z. A prediction model of vessel trajectory based on generative adversarial network. *J. Navig.* **2021**, *74*, 1161–1171. [CrossRef]
36. Chen, P.; Yang, F.; Mou, J.; Chen, L.; Li, M. Regional ship behavior and trajectory prediction for maritime traffic management: A social generative adversarial network approach. *Ocean Eng.* **2024**, *299*, 117186. [CrossRef]

37. Liu, R.W.; Liang, M.; Nie, J.; Yuan, Y.; Xiong, Z.; Yu, H.; Guizani, N. STMGCN: Mobile edge computing-empowered vessel trajectory prediction using spatio-temporal multigraph convolutional network. *IEEE Trans. Ind. Inform.* **2022**, *18*, 7977–7987. [CrossRef]
38. Wang, S.; Li, Y.; Xing, H.; Zhang, Z. Vessel trajectory prediction based on spatio-temporal graph convolutional network for complex and crowded sea areas. *Ocean Eng.* **2024**, *298*, 117232. [CrossRef]
39. Jiang, D.; Shi, G.; Li, N.; Ma, L.; Li, W.; Shi, J. TRFM-ls: Transformer-based deep learning method for vessel trajectory prediction. *J. Mar. Sci. Eng.* **2023**, *11*, 880. [CrossRef]
40. Xue, H.; Wang, S.; Xia, M.; Guo, S. G-Trans: A hierarchical approach to vessel trajectory prediction with GRU-based transformer. *Ocean Eng.* **2024**, *300*, 117431. [CrossRef]
41. International Maritime Organization. International Regulations for Preventing Collisions at Sea, 1972 (COLREGs). Available online: https://www.imo.org/about/conventions/listofconventions/pages/colreg.aspx (accessed on 11 April 2024).
42. Namgung, H.; Ohn, S.W. Fuzzy inference and sequence model-based collision risk prediction system for stand-on vessel. *Sensors* **2022**, *22*, 4983. [CrossRef] [PubMed]
43. Namgung, H.; Kim, J.S. Regional collision risk prediction system at a collision area considering spatial pattern. *J. Mar. Sci. Eng.* **2021**, *9*, 1365. [CrossRef]
44. Sang, L.Z.; Yan, X.P.; Wall, A.; Wang, J.; Mao, Z. CPA calculation method based on AIS position prediction. *J. Navig.* **2016**, *69*, 1409–1426. [CrossRef]
45. Alahi, A.; Goel, K.; Ramanathan, V.; Robicquet, A.; Li, F.-F.; Savarese, S. Social lstm: Human trajectory prediction in crowded spaces. In Proceedings of the IEEE Conference on Computer Vision and Pattern Recognition, Las Vegas, NV, USA, 27–30 June 2016; pp. 961–971.
46. Pei, Z.; Qi, X.; Zhang, Y.; Ma, M.; Yang, Y.H. Human trajectory prediction in crowded scene using social-affinity long short-term memory. *Pattern Recognit.* **2019**, *93*, 273–282. [CrossRef]
47. Namgung, H. Local route planning for collision avoidance of maritime autonomous surface ships in compliance with COLREGs rules. *Sustainability* **2021**, *14*, 198. [CrossRef]
48. Ning, J.; Chen, H.; Li, T.; Li, W.; Li, C. COLREGs-compliant unmanned surface vehicles collision avoidance based on multi-objective genetic algorithm. *IEEE Access* **2020**, *8*, 190367–190377. [CrossRef]
49. Namgung, H.; Kim, J.S. Collision risk inference system for maritime autonomous surface ships using COLREGs rules compliant collision avoidance. *IEEE Access* **2021**, *9*, 7823–7835. [CrossRef]
50. Schuster, M.; Paliwal, K.K. Bidirectional recurrent neural networks. *IEEE Trans. Signal Process.* **1997**, *45*, 2673–2681. [CrossRef]
51. Bahdanau, D.; Cho, K.; Bengio, Y. Neural machine translation by jointly learning to align and translate. *arXiv* **2014**, arXiv:1409.0473.
52. Abadi, M.; Agarwal, A.; Barham, P.; Brevdo, E.; Chen, Z.; Citro, C.; Corrado, G.S.; Davis, A.; Dean, J.; Devin, M.; et al. Tensorflow: Large-scale machine learning on heterogeneous distributed systems. *arXiv* **2016**, arXiv:1603.04467.
53. Sutskever, I.; Vinyals, O.; Le, Q.V. Sequence to Sequence Learning with Neural Networks. In Proceedings of the Annual Conference on Neural Information Processing Systems 2014, Montreal, QC, Canada, 8–13 December 2014; pp. 3104–3112.
54. Gal, Y.; Ghahramani, Z. A theoretically grounded application of dropout in recurrent neural networks. *Adv. Neural Inf. Process. Syst.* **2016**, *29* , 1019–1027.
55. Kendall, A.; Gal, Y. What uncertainties do we need in bayesian deep learning for computer vision? *Adv. Neural Inf. Process. Syst.* **2017**, *30* , 5580–5590.
56. Guo, Z.; Qiang, H.; Xie, S.; Peng, X. Unsupervised knowledge discovery framework: From AIS data processing to maritime traffic networks generating. *Appl. Ocean Res.* **2024**, *146*, 103924. [CrossRef]
57. Tang, H.; Yin, Y.; Shen, H. A model for vessel trajectory prediction based on long short-term memory neural network. *J. Mar. Eng. Technol.* **2022**, *21*, 136–145. [CrossRef]
58. Vaswani, A.; Shazeer, N.; Parmar, N.; Uszkoreit, J.; Jones, L.; Gomez, A.N.; Kaiser, L.; Polosukhin, I. Attention Is All You Need. In Proceedings of the 31st Conference on Neural Information Processing Systems (NIPS 2017), Long Beach, CA, USA, 4–9 December 2017.

Disclaimer/Publisher's Note: The statements, opinions and data contained in all publications are solely those of the individual author(s) and contributor(s) and not of MDPI and/or the editor(s). MDPI and/or the editor(s) disclaim responsibility for any injury to people or property resulting from any ideas, methods, instructions or products referred to in the content.